



Spatio-temporal variability and controlling factors for postglacial erosion dynamics in the Dora Baltea catchment (western Italian Alps)

Elena Serra^{1,2}, Pierre G. Valla^{3,1,2}, Romain Delunel⁴, Natacha Gribenski^{1,2}, Marcus Christl⁵, Naki Akçar¹

¹Institute of Geological Sciences, University of Bern, Bern, 3012, Switzerland

5 ²Oeschger Centre for Climate Change Research, University of Bern, Bern, 3012, Switzerland.

³University Grenoble Alps, University Savoie Mont Blanc, CNRS, IRD, IFSTTAR, ISTERre, Grenoble, 38000, France

⁴Université Lumière Lyon 2, CNRS, UMR 5600 EVS, F-69635, France

⁵Laboratory of Ion Beam Physics, Swiss Federal Institute of Technology Zurich (ETHZ), Zurich, 8093, Switzerland

Correspondence to: Elena Serra (elena.serra@geo.unibe.ch)

10 **Abstract.** Disentangling the influence of bedrock erodibility from the respective roles of climate, topography and tectonic forcing on catchment denudation is often challenging in mountainous landscapes due to the diversity of geomorphic processes in action and of spatial/temporal scales involved. The Dora Baltea catchment (western Italian Alps) appears the ideal setting for such investigation, since its large drainage system, extending from the Mont Blanc Massif to the Po Plain, cuts across different major litho-tectonic units of the western Alps, whereas this region has experienced homogeneous climatic conditions and glacial history throughout the Quaternary. We acquired new ¹⁰Be-derived catchment-wide denudation rates from 18 river-sand samples collected both along the main Dora Baltea river and at the outlet of its main tributaries. The inferred denudation rate results vary between 0.2 and 0.9 mm/yr, consistent with values obtained across the European Alps by previous studies. Spatial variability in denudation rates was statistically compared with topographic, environmental and geologic metrics. ¹⁰Be-derived denudation records do not correlate with the distribution of modern precipitation and rock geodetic uplift. We find, rather, that catchment topography, in turn conditioned by bedrock erodibility (litho-tectonic origin) and glacial overprint, has the main influence on denudation rates. We calculated the highest denudation rate for the Mont Blanc Massif, whose granitoid rocks and long-term tectonic uplift support steep slopes and high relief and thus favour intense glacial/periglacial processes and recurring rock fall events. Finally, our results, in agreement with modern sediment budgets, demonstrate that the high sediment input from the Mont Blanc catchment dominates the Dora Baltea sediment flux, explaining the constant low ¹⁰Be concentrations measured along the Dora Baltea course even downstream the multiple junctions with tributary catchments.

1 Introduction

The use of *in-situ* ¹⁰Be concentrations measured in river sediments to quantify catchment-wide denudation rates over centennial to millennial time scale is now well-established (e.g. Granger and Schaller, 2014). ¹⁰Be concentrations are measured at the outlet of the studied basin and are inversely correlated to mean catchment denudation rate (von Blanckenburg, 2005).

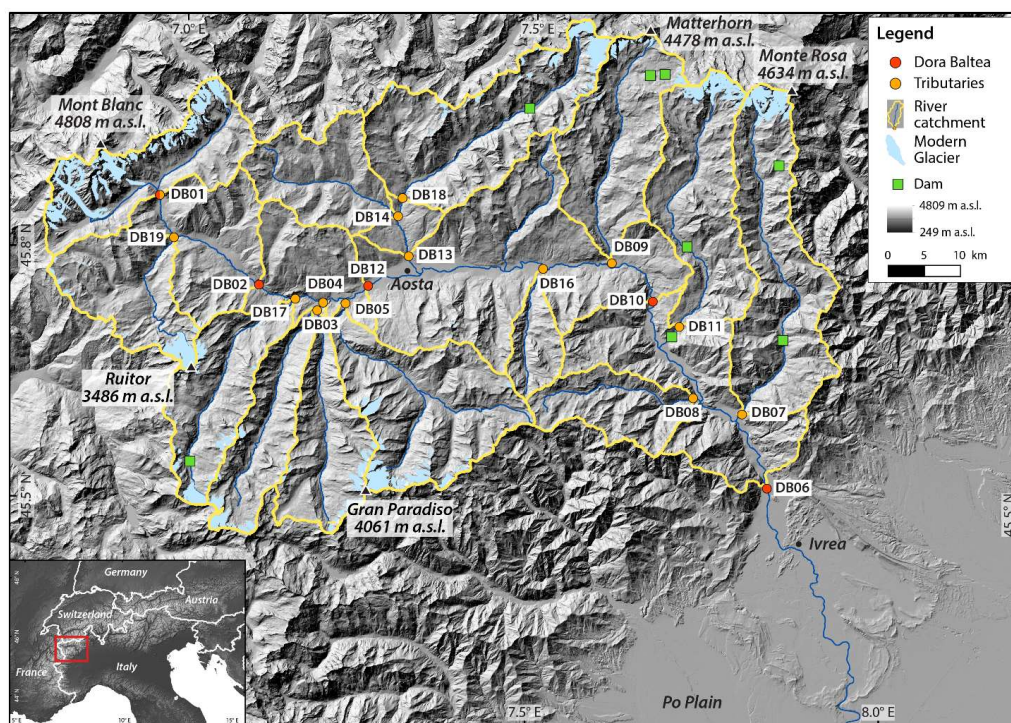
30 Widespread research investigation has used this technique to estimate catchment denudation around the globe (see reviews in Portenga and Bierman, 2011; Willenbring et al., 2013; Codilean et al., 2018) and in mountain belts such as the European Alps (Delunel et al., 2020 and references therein), with the aim of illustrating the controlling mechanisms on recent (10²-10⁵ years) erosion dynamics and assessing the respective roles of climate, tectonics or even anthropogenic forcing.

In mountainous areas, the climatic imprint on the Earth's surface denudation has been recognized over both long and short timescales. Over the Late Cenozoic to Quaternary, temperature fluctuations, increased precipitation and glaciations significantly modified catchment morphology (Peizhen et al., 2001; Herman et al., 2013) (i.e. increased slope steepness and relief; e.g. Valla et al., 2011), which in turn triggered a postglacial erosional response (Norton et al., 2010; Valla et al., 2010; Glotzbach et al., 2013; Dixon et al., 2016). Over recent timescales, climate also exerts a control on denudation rates through precipitation and associated runoff (Moon et al., 2011; Bookhagen and Strecker, 2012) and by governing temperature/precipitation-dependent glacial and periglacial erosion processes (e.g. Delunel et al., 2010; Deline et al., 2014).



Alternatively, other studies have shown a dominant litho-tectonic control on denudation rates (e.g. Cruz Nunes et al., 2015). Rock-uplift and denudation rates are strongly coupled, with (1) erosional unloading driving uplift through isostatic rebound (Wittmann et al., 2007; Champagnac et al., 2009), and (2) tectonic rock uplift itself conditioning denudation rate by building new topographic gradient (Godard et al., 2014). Bedrock lithology also governs denudation through its erosional resistance
45 (erodibility, Kühni and Pfiffner, 2001). More resistant lithologies have contrasting potential controls on denudation, (1) either decreasing denudation rates because of rock-mechanical strength (Scharf et al., 2013), (2) or promoting higher denudation rates by sustaining steep topography instead (Norton et al., 2011).

In the European Alps, the large-scale compilation of catchment-wide denudation rates by Delunel et al. (2020) highlighted (1) the first-order correlation between topographic slope (derived from glacial impact on Alpine topography) and denudation rate,
50 (2) the absence of control of modern climate on denudation patterns and (3) a significant correlation between rock uplift and denudation for >100-km² catchments. This compilation also pointed at a rather weak control of lithology on denudation, with the lowest rates in the low-elevation foreland areas (with clastic sedimentary lithology) and highest rates in the high-elevation crystalline parts (with gneissic, granitic or metamorphic lithologies) within the core of the Alps. This trend, however, was not investigated further, since, at the scale of the European Alps, it appeared difficult to disentangle the relative influence of
55 bedrock erodibility, topography and tectonic forcing on denudation rate as these are closely interrelated. Our study thereby aims to further explore the potential links and controls between climatically-driven topography, tectonic uplift and bedrock erodibility on the efficiency of erosion processes by investigating spatial variability of ¹⁰Be-derived denudation rates within the Dora Baltea (DB) catchment (western Italian Alps; Fig. 1). The DB catchment appears the ideal setting for this investigation, since its large drainage system, extending from the Mont Blanc Massif (4808 m a.s.l.) to the Po Plain (around
60 200 m a.s.l.), cuts across the main litho-tectonic units of the western Alps (Fig. 2). Relatively similar climatic conditions and glacial history but variable bedrock lithology and geodetic uplift within the DB catchment and its tributaries allow us to assess how spatial variability in bedrock erodibility between litho-tectonic units may participate in controlling catchment topography and ¹⁰Be-derived denudation rates.





65 **Figure 1:** Study area with investigated Dora Baltea (DB) and main tributary river catchments (mosaic DEM from Regione Autonoma Valle
d'Aosta, Regione Piemonte, swisstopo, and Institut Géographique National). Red and yellow circles indicate locations of river-sediment
samples collected along the Dora Baltea river and at the outlet of the main river tributaries, respectively (for DB01 red-yellow circle as both
along the Dora Baltea and considered as an individual tributary). Solid yellow lines delimit the catchments upstream of each sampling
location (sample names indicated in white box). Present-day glaciers (GlaRiskAlp Project, <http://www.glariskalp.eu>), main topographic
70 peaks and dams are indicated. Inset shows location of the DB catchment (red open box) within the European Alps.

2 Study area

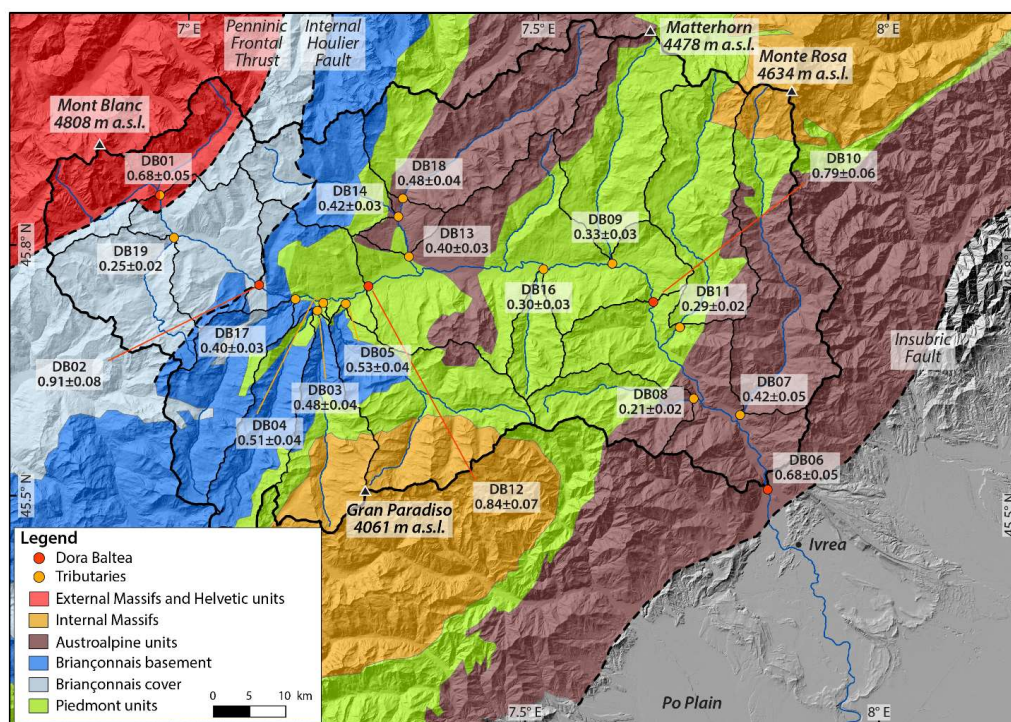
The Dora Baltea (DB) catchment is a large drainage system of ~3900 km² located in the western Italian Alps (Fig. 1). Over a
170-km long distance, the DB river flows NW-SE from the Mont Blanc Massif to the Po Plain, and drains several tributary
valleys (13 of which are investigated in this study) connected to major 4000-m Alpine peaks (e.g. Mont Blanc, Monte Rosa,
75 Matterhorn and Gran Paradiso; Fig. 1). Present-day mean annual temperatures range from -10°C (high elevation zones) to
15°C (valley bottoms) within the DB basin (Regione Autonoma Valle d'Aosta, 2009). Precipitations are spatially variable
across the DB catchment, with higher mean annual values observed in the Mont Blanc Massif (around 1800 mm/yr) compared
to the north-western and southern sectors of the DB catchment (around 1400 mm/yr for Matterhorn and Monte Rosa area, and
around 1150 mm/yr in the Grand Paradiso), and semi-arid conditions prevailing in the central part of the DB valley (mean
80 annual precipitation of 400-500 mm/yr; Isotta et al., 2014). Present-day glaciers cover 3.6% of the total DB area, and are
distributed within the upstream high-elevation parts of DB tributary catchments (terminus glacier elevations ranging from
2601 to 2800 m a.s.l. in 2005; Diolaiuti et al., 2012).

The geology of the DB catchment is complex, since the DB drainage network cuts across the main litho-tectonic units of the
85 western Alps, recording the long-term collisional history between the European and Adriatic plates (e.g. Dal Piaz et al., 2008;
Perello et al., 2008; Polino et al., 2008; Fig. 2). West of the Penninic Frontal Thrust, the European basement is exposed in the
granitoid of the Mont Blanc External Massif and its Helvetic sedimentary cover. Bedrock units belonging to the thinned
European crust (gneisses and schists of the Briançonnais basement and its terrigenous to carbonate metasedimentary cover,
high-pressure gneisses of the Internal Massifs), the Tethyan oceanic crust (meta-ophiolite and calcschists of the Piedmont
90 units) and the Adriatic margin (Austroalpine gneisses and eclogitic micaschists) are exposed roughly from NW to SE across
the axial belt (delimited by the Penninic Frontal Thrust to the NW and the Insubric Fault to the SE; Fig. 2). Long-term (10⁶-
10⁷ years) exhumation rates estimated from bedrock apatite fission-track dating are higher in the western sector of the DB
catchment (0.4-0.7 km/Myr for the External zones, west of Internal Houiller Fault; Fig. 2) than in the east (0.1-0.3 km/Myr for
the Internal zones, i.e. between the Internal Houiller and the Insubric Faults, Malusà et al., 2005; Fig. 2). Similarly, modern
95 geodetic rock uplift appears spatially variable within the DB catchment, with rates up to 1-1.6 mm/yr in the Monte Rosa, Mont
Blanc and Ruitor areas, around 0.6-0.7 mm/yr in the axial belt and in the Gran Paradiso Massif, while decreasing to 0.2 mm/yr
in the Po plain (Sternai et al., 2019).

The DB catchment was repeatedly glaciated during the Quaternary, with the extensive DB glacial system (~3000 km², >1000
m thick; Serra et al., in revision) abandoning the Po Plain after the Last Glacial Maximum (LGM, ca. 26-19 ka; Clark et al.,
100 2009), and the tributary glaciers already retreated in their upper valley catchments during the Lateglacial climatic oscillations
(14-12 ka; Baroni et al., 2021; Serra et al., in revision). As shown by present-day topography (Fig. 1), postglacial fluvial
dissection and hillslope processes following deglaciation have locally re-shaped the glacial landscape, with the development
of V-shape valleys profiles and the spread of large alluvial fans and sediment deposits along the main valleys. Both long-term
(10⁶-10⁷ years), short-term (10²-10⁵ years) and modern (10¹-10² years) catchment-wide denudation rates, inferred respectively
105 from bedrock apatite fission-track dating (Malusà et al., 2005), detrital apatite fission-track data (Resentini and Malusà, 2012)
and river sediment load budgets (Bartolini et al., 1996; Vezzoli, 2004; Bartolini and Fontanelli, 2009), indicate higher erosion
in the Mont Blanc External Massif (ca. 0.7 mm/yr) than in the rest of the catchment (≤0.3 mm/yr). For the entire DB catchment,



¹⁰Be-derived denudation rate of 0.6 mm/yr was obtained (sample T12 of Wittmann et al., 2016, approximately same location as our sample DB06 on Fig. 1).



110

Figure 2. Simplified litho-tectonic map of the study area with output catchment-wide denudation rates (mm/yr) reported at sampling locations (catchment boundaries in solid black lines). Major litho-tectonic domains and structural features (dashed lines) of the Western European Alps are shown (modified map after Resentini and Malusà, 2012). Output catchment-wide denudation rates are corrected for topographic, LIA-glacier and snow shielding, and for quartz-content (see text and Table 1 for details).

115 3 Methods

3.1 ¹⁰Be-derived catchment-wide denudation rates

Eighteen river-sand samples were collected within the DB catchment, 5 along the main DB river and 13 at the outlet of the main tributaries (Fig. 1). Around 20-50 g of pure quartz were extracted from the 250-400 μm grain size fraction, following sieving, magnetic separation and leaching in diluted HCl, H₃PO₄ and HF (detailed protocol reported in Akçar et al., 2017).

120 The purified quartz was dissolved in concentrated HF after addition of around 200 μg of ⁹Be carrier (Table S1), and Be extraction was performed through anion and cation exchange column chemistry (Akçar et al., 2017). Measurements of ¹⁰Be/⁹Be ratios were performed at ETH Zürich with the MILEA AMS system (Maxeiner et al., 2019), and normalized to the ETH in-house standards S2007N and S2010N (isotope ratios 28.1 × 10⁻¹² and 3.3 × 10⁻¹², respectively; Christl et al., 2013). Calculated ¹⁰Be concentrations (Table 1) were corrected using a full process blank ¹⁰Be/⁹Be ratio of 2.96 ± 0.32 × 10⁻¹⁵.

125 In order to compute catchment-wide denudation rates, catchment spatially-averaged ¹⁰Be production rates were calculated, using Basinga 'Production rates' GIS tool (Charreau et al., 2019), with a 35-m resolution DEM from Regione Autonoma Valle d'Aosta and Regione Piemonte as input for catchment topography. The ¹⁰Be surface production rate at each DEM cell of the studied catchments was calculated based on a ¹⁰Be production rate at sea-level and high-latitude (SLHL) of 4.18 ± 0.26 at g⁻¹ yr⁻¹ (Martin et al., 2017) scaled with the Lal/Stone time-dependent scaling model (Lal, 1991; Stone, 2000), integrating



130 corrections for atmospheric pressure and geomagnetic field fluctuations according to the ERA-40 reanalysis database (Uppala et al., 2005) and the Muscheler's VDM database (Muscheler et al., 2005), respectively.

Catchment-averaged production rates were corrected for (1) topographic shielding, (2) quartz-content, (3) LIA-glacier cover, and (4) snow shielding (Charreau et al., 2019). Catchment topographic shielding was computed with the 'toposhielding' Topotoolbox function (Schwanghart and Scherler, 2014), following the method of Dunne et al. (1999) and Codilean (2006).

135 Based on the 1/100,000- and 1/250,000-scale digital geological maps from Regione Autonoma Valle d'Aosta and Regione Piemonte, respectively, we mapped and excluded from the ^{10}Be production-rate calculation catchment areas covered by mafic and non-siliceous sedimentary (carbonate) bedrocks (Fig. S1), based on the assumption that they do not provide (or to a minor extent) quartz grains to the fluvial routing system. Crystalline bedrocks and Quaternary deposits (Fig. S1) were instead considered as quartz-bearing lithologies in our approach. In addition, we excluded areas with slope $< 3^\circ$, assuming that they

140 are likely not linked to the stream network or act as storage/transfer areas and therefore do not reflect catchment denudation (Fig. S1; Delunel et al., 2010). In order to estimate shielding correction due to glacier cover, ^{10}Be production rates were set to null for areas covered by Little Ice Age (LIA, 1250-1860 CE) glaciers (GlaRiskAlp Project, <http://www.glariskalp.eu>; Fig. S1), this conservative approach assuming sufficient ice thickness for complete cosmic-ray shielding (e.g. Delunel et al., 2010; Wittmann et al., 2007). Shielding correction factors for snow cover were calculated as function of the average elevation for each individual catchment, by applying an empirical model reported in Delunel et al. (2020) that allows to predict snow-shielding factors as a function of elevation for the European Alps. The snow-shielding correction factors were then combined to topographic-shielding corrections in a single raster for the DB catchment.

145 Catchment-wide denudation rates were then obtained using the previously-calculated catchment-averaged ^{10}Be production rates and the measured ^{10}Be concentrations (Table 1), using the Basinga 'Denudation rates' GIS tool (Charreau et al., 2019).

150 3.2 Topographic, environmental and geological metrics

In order to investigate potential drivers conditioning the observed spatial variability in catchment-wide denudation rates within the DB catchment, we performed topographic analyses, and extracted environmental and geological variables for each investigated tributary catchment through an ArcGIS-Matlab routine (Delunel et al., 2020).

155 Topographic analyses were conducted using a 35-m resolution DEM (Regione Autonoma Valle d'Aosta and Regione Piemonte). We calculated drainage area, mean elevation, mean slope, percentage of slopes steeper than 40° , geophysical relief, and hypsometric integral for each individual catchment (Table 2). For slope analyses, the 'gradient8' Topotoolbox function was used (Schwanghart and Scherler, 2014), returning the steepest downward gradient of the 8-connected neighbouring cells of the DEM. The percentage of catchment slope steeper than 40° was calculated as indicative of the areal proportion of oversteepened threshold landscape (DiBiase et al., 2012). The geophysical relief (i.e. averaged elevation differences between a surface connecting highest topographic points and the current topography; Small and Anderson, 1998) was calculated in

160 ArcGIS using a 5-km radius sampling window, and can be used as an indicator of past landscape change (i.e. high geophysical relief may indicate increased relief from locally increased erosion; Champagnac et al., 2014). The hypsometric integral was computed based on Eq. 1 from Brocklehurst and Whipple (2004) and is inversely related to the stage of landscape evolution (i.e. more evolved landscapes, whose high-elevation areas have been eroded, have lower hypsometric integrals).

165 In addition, we extracted catchment-averaged values of the following environmental variables. Averaged annual precipitation for each catchment was obtained from the 5-km resolution grid of mean annual Alpine precipitation from Isotta et al. (2014), in order to investigate the potential influence of modern precipitation/runoff on erosion dynamics. Percentage of bare-rock area was estimated from the extent of class 30 ("bare bedrock") of the 100-m resolution CORINE Land Cover Inventory (2018), to consider if catchment areas with null to low soil/vegetation cover are more subject to erosion. LIA-glacier areal cover was calculated based on the LIA-glacier extent mapped within the GlaRiskAlp Project (<http://www.glariskalp.eu>), in

170 order to investigate the influence of modern to historical glacial and periglacial processes on ^{10}Be -derived denudation (Delunel



et al., 2010). Mean LGM ice-thickness and areal percentage of each catchment above the LGM Equilibrium Line Altitude (ELA) were estimated by using the LGM paleo-glacier reconstruction of the DB system (70-m resolution, ELA at 2103 m a.s.l.; Serra et al., in revision), both metrics potentially giving indication on the LGM glacial imprint on topography and subsequent potential for postglacial erosion response (Norton et al., 2010; Salcher et al., 2014; Delunel et al., 2020).

Lastly, we extracted geological variables for studied catchments. Based on the simplified litho-tectonic map of the DB catchment (Fig. 2), modified after Resentini and Malusà (2012), we estimated the relative proportion of the different litho-tectonic units within each catchment. Catchment-averaged geodetic uplift rates were as well considered using the 30-km resolution interpolation grid from Sternai et al. (2019), here downscaled to 600-m resolution grid (Delunel et al., 2020).

180 4 Results

4.1 Spatial variability in catchment-wide denudation rates

Calculated catchment-wide ^{10}Be production rates and derived denudation rates vary according to the applied production-rate correction factors (Table S2). Uncorrected denudation rates (i.e. including only mean catchment topographic shielding and excluding areas with slope $<3^\circ$) range between 0.27 ± 0.02 and 1.49 ± 0.13 mm/yr, while rates obtained by applying all corrections vary between 0.21 ± 0.02 and 0.91 ± 0.08 mm/yr (Table 1 and Fig. 2). Significant production-rate corrections were obtained when taking into account snow shielding and LIA-glacier cover (up to 17 and 42% reduction compared to uncorrected ^{10}Be production/denudation rates, respectively), especially for catchments with high mean elevations and associated high LIA-glacier coverage (Table 2). Lower corrections were obtained when considering quartz-content (maximum 10% reduction in output ^{10}Be production/denudation for catchments DB08 and 11, where relatively abundant sedimentary and mafic bedrocks occur; Fig. S1). All corrections combined together lead to reduction in ^{10}Be production/denudation rates of 16-53% compared to the uncorrected estimates. Hereafter, we consider ^{10}Be production/denudation rates obtained by applying all corrections (Table 1 and Fig. 2), in order to maintain a conservative approach as in the recent Alpine compilation study (Delunel et al., 2020).

Sample	Location WGS 84 (°N/°E)	Elevation (m a.s.l.)	^{10}Be concentration ($\times 10^4$ at g^{-1}) ^a	Topographic shielding ^b	Mean production rate (at $\text{g}^{-1} \text{yr}^{-1}$) ^c		Denudation rate (mm yr^{-1}) ^d		Apparent age (yr)	
					Uncorr.	Corr.	Uncorr.	Corr.	Uncorr.	Corr.
DB01	45.8040/ 6.9653	1230	1.29 ± 0.07	0.92	29.4	13.7	1.45 ± 0.11	0.68 ± 0.05	415	885
DB02	45.7167/ 7.1101	783	1.08 ± 0.07	0.94	25.1	15.3	1.40 ± 0.13	0.91 ± 0.08	403	657
DB03	45.6925/ 7.1935	699	2.35 ± 0.14	0.94	28.6	18.0	0.76 ± 0.06	0.48 ± 0.04	789	1251
DB04	45.7003/ 7.2019	664	2.20 ± 0.11	0.94	27.5	17.8	0.78 ± 0.06	0.51 ± 0.04	768	1178
DB05	45.7001/ 7.2337	638	2.05 ± 0.10	0.95	27.8	17.4	0.85 ± 0.06	0.53 ± 0.04	709	1131
DB06	45.5228/ 7.8375	251	1.54 ± 0.08	0.95	22.6	16.1	0.94 ± 0.07	0.68 ± 0.05	636	887
DB07	45.5962/ 7.7956	325	2.25 ± 0.26	0.95	22.2	15.3	0.61 ± 0.07	0.42 ± 0.05	977	1413
DB08	45.6118/ 7.7310	373	4.85 ± 0.21	0.96	20.2	15.9	0.27 ± 0.02	0.21 ± 0.02	2263	2859
DB09	45.7352/ 7.6124	465	3.34 ± 0.18	0.96	24.4	17.5	0.46 ± 0.04	0.33 ± 0.03	1305	1823
DB10	45.7079/ 7.6713	375	1.35 ± 0.07	0.95	23.5	16.5	1.12 ± 0.09	0.79 ± 0.06	535	760



DB11	45.6830/ 7.7115	546	3.47±0.20	0.96	24.5	16.0	0.44±0.04	0.29±0.02	1352	2058
DB12	45.7183/ 7.2651	594	1.26±0.08	0.95	25.6	16.4	1.30±0.11	0.84±0.07	460	715
DB13	45.7482/ 7.3224	753	2.79±0.12	0.95	24.4	17.2	0.56±0.04	0.40±0.03	1075	1518
DB14	45.7882/ 7.3061	600	2.83±0.13	0.96	22.1	18.5	0.50±0.04	0.42±0.03	1194	1426
DB16	45.7386/ 7.4292	524	3.88±0.35	0.94	23.6	18.7	0.38±0.04	0.30±0.03	1574	1989
DB17	45.7039/ 7.1622	689	2.71±0.13	0.95	27.2	17.3	0.63±0.05	0.40±0.03	956	1497
DB18	45.7039/ 7.1622	689	2.30±0.12	0.94	27.0	17.2	0.75±0.06	0.48±0.04	803	1255
DB19	45.7619/ 6.9873	1005	4.19±0.15	0.96	25.8	16.0	0.39±0.03	0.25±0.02	1531	2448

Table 1: River-sediment sample locations, measured ^{10}Be concentrations, calculated mean catchment ^{10}Be production rates, and output denudation rates and apparent ages. Production rate estimates (and derived denudation rates / apparent ages) are provided for (1) topographic shielding correction (column labeled “Uncorr.”) and (2) including corrections for topographic shielding, snow and LIA-glacier shielding and for quartz-content (column labelled Corr.). Mean catchment ^{10}Be production rates (and derived catchment denudation rates) obtained by applying each individual correction are reported in Table S2.

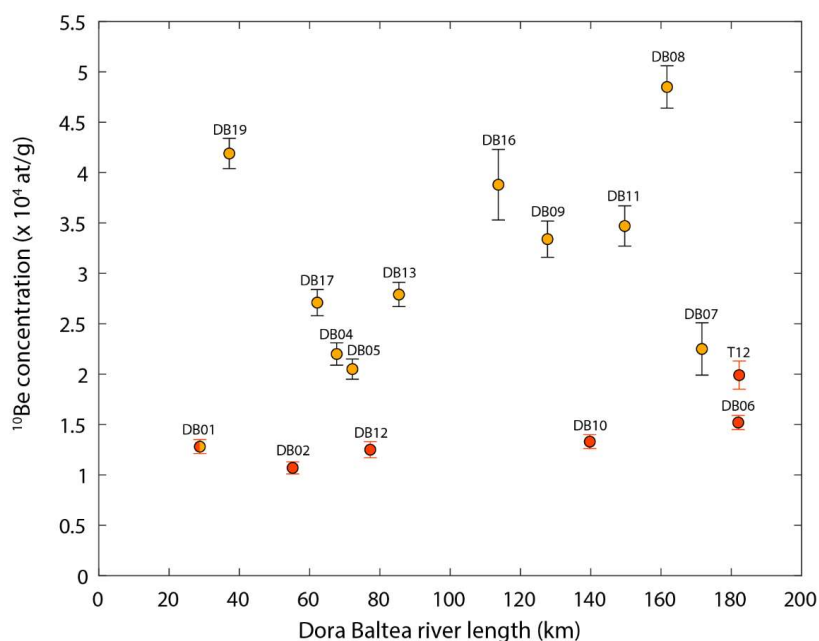
^a ^{10}Be measurements were calibrated against ETH in-house standards S2007N and S2010N (isotope ratios 28.1×10^{-12} and 3.3×10^{-12} , respectively; Christl et al., 2013). Calculated ^{10}Be concentrations were corrected for full process blank $^{10}\text{Be}/^9\text{Be}$ ratio of $2.96 \pm 0.32 \times 10^{-15}$. Additional analytical data are reported in Table S1.

^b Catchment topographic shielding was computed with the ‘toposhielding’ Topotoolbox function (Schwanghart and Scherler, 2014, after Dunne et al., 1999 and Codilean, 2006).

^c Catchment-averaged ^{10}Be production rates were calculated with Basinga (Charreau et al., 2019), based on SLHL total ^{10}Be production rate of 4.18 ± 0.26 at $\text{g}^{-1} \text{yr}^{-1}$ (Martin et al., 2017) and the Lal/Stone time-dependent scaling model (Lal, 1991; Stone, 2000). Neutron, slow and fast muons are assumed to contribute respectively 98.86, 0.87 and 0.27% to the total ^{10}Be production rate (Charreau et al., 2019, after Braucher et al., 2011, and Martin et al., 2017).

^d ^{10}Be -derived catchment denudation rates were calculated with Basinga (Charreau et al., 2019), using default attenuation length values of 160, 1500 and 4320 g cm^{-2} , for neutrons, slow muons, and fast muons, respectively (Charreau et al., 2019, after Braucher et al., 2011), and assuming a rock density of 2.7 g cm^{-3} . Denudation-rate uncertainties are estimated only based on values and relative errors of ^{10}Be concentrations and cosmogenic production rates from neutron and muons (Eq. 5 in Charreau et al., 2019).

^e Apparent ages represent the time needed to erode one absorption depth scale ($\sim 0.6 \text{ m}$ in bedrock; von Blanckenburg, 2005) and are given as mean estimates (no uncertainty propagated).





- 215 **Figure 3:** Downstream evolution of river-sand ^{10}Be concentrations in the Dora Baltea (DB) catchment. Data are plotted versus distance from the main DB source (upper Val Veny, right tributary upstream DB01). In red are samples collected along the main DB river, in yellow are samples at the outlet of tributaries (Fig. 1). ^{10}Be concentration of sample T12 from Wittmann et al. (2016) is also shown for discussion. Samples DB03 and DB14 and 18 are omitted since they are in turn tributaries of catchments DB04 and DB13, respectively, and do not directly connect to the main DR river.
- 220 The highest denudation rates (0.7-0.9 mm/yr) were obtained from riverine samples collected along the main DB river (DB01, 02, 12, 10, 06), showing a slightly-decreasing trend in denudation rate with the river distance (apart from DB01; Fig. 2). ^{10}Be concentrations measured in these samples are the lowest and overall constant along the DB course (around 1.2×10^4 at/g; Fig. 3). Within tributary catchments, with the exception of sample DB01, ^{10}Be concentrations are higher ($2.0\text{-}4.9 \times 10^4$ at/g; Fig. 3), and calculated denudation rates are lower, generally within 0.4-0.5 mm/yr and down to 0.2-0.3 mm/yr for some catchments
- 225 (DB08, 09, 11, 16 and 19; Fig. 2).

4.2 Catchment metrics and denudation rates

Results of catchment topographic analyses, along with estimates of environmental and geological metrics, are reported in Table 2. As for calculated catchment-wide denudation rates, DB01 (Mont Blanc Massif) also appears as an end-member with maximum values in most of the reported metrics (Table 2).

230

Catchment	Drainage area (km ²)	Mean elevation (m a.s.l.)	Mean slope (°)	Relative abundance of slopes > 40° (%)	Geophysical relief (5-km, m)	Hypsometric integral	Mean annual precipitation (mm)	Relative abundance of bare-rock (%)	LIA glacier cover (%)	Mean LGM ice-thickness (m)	Basin area above LGM ELA (%)	Mean geodetic rock uplift (mm yr ⁻¹)
DB01	189	2563	31.5	31.6	1628	0.38	1763	33.8	34.3	492	75	1.08
DB02	496	2289	28.4	28.3	1276	0.38	1481	24.9	19.1	573	63	1.19
DB03	147	2506	29.2	31.0	1206	0.54	1083	36.3	14.9	436	77	0.89
DB04	279	2445	28.5	30.7	1141	0.53	1073	35.8	15.8	447	74	0.99
DB05	257	2452	29.3	27.7	1138	0.53	1041	32.0	15.0	414	74	0.67
DB06	3321	2083	27.7	25.8	1191	0.41	1128	19.5	9.7	513	53	0.93
DB07	278	2057	30.0	26.6	1093	0.41	1342	11.5	7.5	314	46	0.69
DB08	108	1962	28.5	27.4	951	0.57	1156	8.4	0.9	229	45	0.50
DB09	207	2225	25.7	21.2	1205	0.45	1084	18.7	10.1	306	61	1.31
DB10	2464	2155	28.2	26.6	1210	0.40	1111	22.8	11.2	546	58	1.02
DB11	226	2209	26.9	21.6	1142	0.45	1080	16.7	9.6	322	57	1.02
DB12	1310	2317	28.1	27.2	1179	0.41	1215	27.3	16.0	515	66	1.02
DB13	450	2236	28.9	28.1	1143	0.46	1148	26.4	10.1	559	61	1.10
DB14	141	2107	27.1	20.5	1078	0.46	1273	13.3	1.0	559	53	0.93
DB16	54	2219	30.4	30.5	1068	0.57	946	24.2	2.3	371	65	0.68
DB17	158	2422	27.7	24.2	1040	0.57	1053	32.0	20.2	428	74	1.24
DB18	277	2411	30.6	33.4	1135	0.48	1129	36.0	15.9	502	72	1.21
DB19	148	2346	25.1	22.8	876	0.55	1273	26.5	19.0	485	73	1.40

235 **Table 2:** Topographic, environmental and geological metrics extracted for the studied catchments (upstream of sampling locations for ^{10}Be analysis on riverine sediments). Topographic metrics were extracted from a 35-m resolution DEM (Regione Autonoma Valle d'Aosta and Regione Piemonte). Other catchment metrics include mean annual precipitation (Isotta et al., 2014), relative catchment bare-rock area from CORINE Land Cover Inventory (2018), LIA glacier extent from GlaRiskAlp Project (<http://www.glariskalp.eu>). Mean catchment LGM ice-thickness and LGM ELA (2103 m a.s.l.) are taken from Serra et al. (in revision). Finally, catchment-averaged geodetic uplift is extracted from Sternai et al. (2019).

We compared ^{10}Be -derived catchment denudation rates against topographic, environmental and geological metrics and evaluated the statistical significance of investigated linear correlations (p-value and R²; Figs. 4 and 5, Table S3). Samples along the main DB river (downstream of DB01, i.e. DB02, 12, 10, 06; Fig. 2) were excluded from the investigated correlations since their apparent denudation rates are potentially affected by cumulative drainage and sediment mixing along the DB course. Correlations were calculated both including and excluding sample DB01, in order to assess whether DB01 strongly influences

240



the derived correlations as a potential outlier. Significant linear correlations (i.e. p -value < 0.05) both with and without DB01 were obtained between catchment denudation rates and topographic metrics, including mean elevation (Fig. 4A) and 5-km geophysical relief (Fig. 4C). Significant linear correlations between catchment denudation rates and slopes (Fig. 4B) or proportions of oversteepened slopes (Table S3) were only found when including DB01. In addition, we found statistical linear correlations for environmental metrics such as the relative abundance of bare bedrock (Fig. 5B), and the percentage of area covered by LIA glaciers (only including DB01; Fig. 5C).

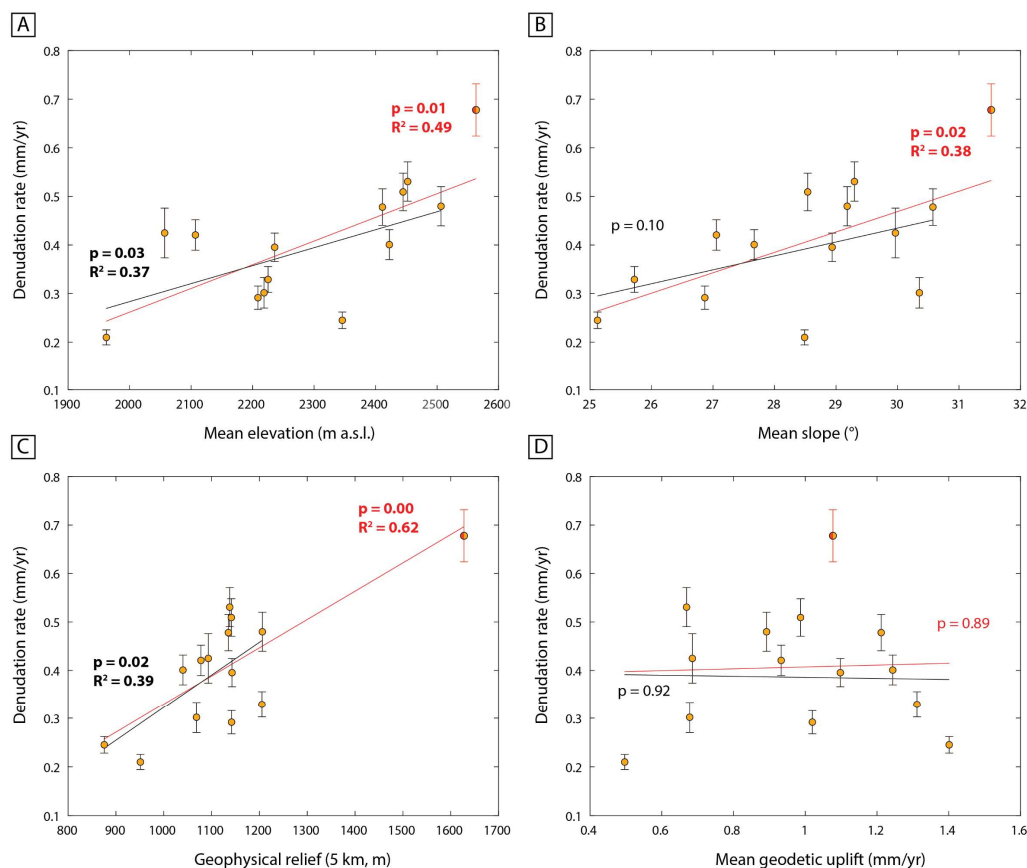


Figure 4: Correlations between tributary-catchment denudation rates and mean catchment (A) elevation, (B) slope, (C) 5-km geophysical relief, and (D) geodetic uplift. Correlations have been calculated including or not sample DB01 (red and black lines, respectively; see main text for discussion). Correlation coefficients (p -value and R^2) are reported for each plot with significant trend (p -value < 0.05). R^2 is not reported for non-significant correlations (p -value > 0.05).

Non-significant correlations (p -value ≥ 0.05) were observed between catchment denudation rates and drainage areas (Table S3), hypsometric integrals (Table S3), mean annual precipitation values (Fig. 5A), and mean geodetic uplift rates (Fig. 4D). Finally, only weak linear correlations (p -value ~ 0.06 - 0.08 , including DB01) can be observed between catchment denudation rates and LGM glacial metrics (mean LGM ice-thickness and catchment proportion above LGM ELA, Table S3 and Fig. 5D).

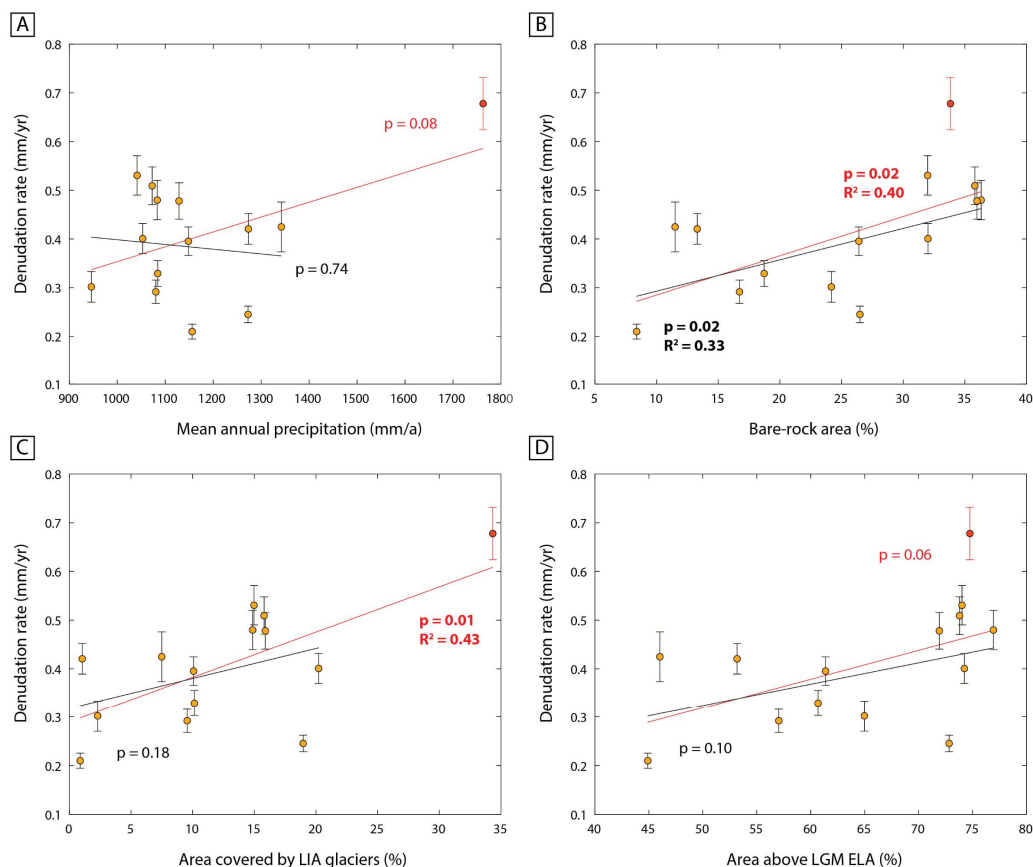
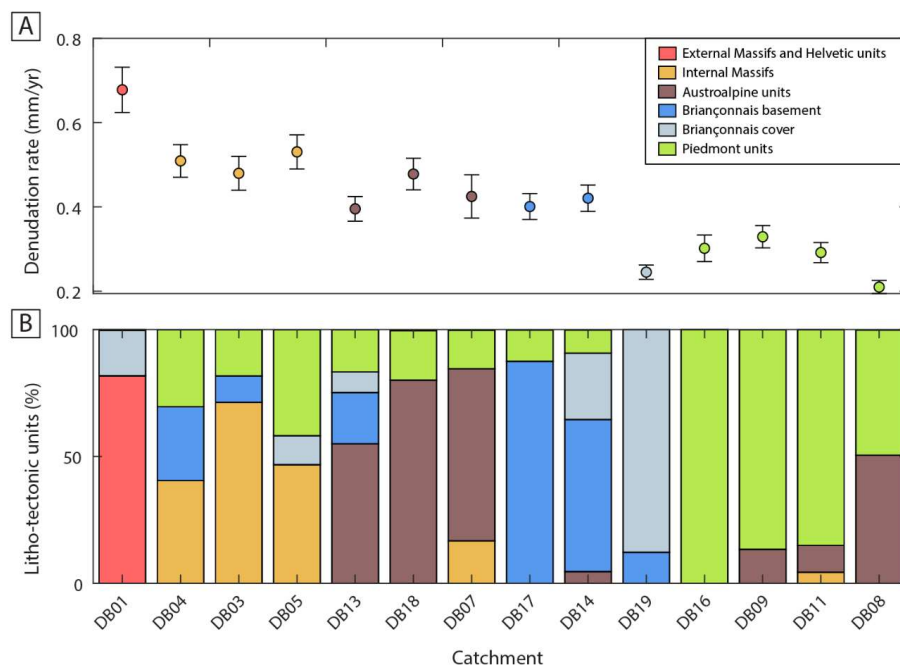


Figure 5: Correlations between tributary-catchment denudation rates and catchment (A) mean annual precipitation, (B) relative bare-bedrock area, (C) relative area covered by LIA glaciers, and (D) relative area above LGM ELA (2103 m a.s.l.). Correlations have been calculated including or not sample DB01 (red and black lines, respectively; see text for discussion). Correlation coefficients (p-value and R^2) are reported for each plot with significant trend (p-value < 0.05). R^2 is not reported for non-significant correlations (p-value > 0.05).

4.3 Litho-tectonic units and denudation rates

In addition to catchment metrics, we explored the potential influence of bedrock properties on the efficiency of geomorphic processes and catchment denudation rates by analysing the correlation between tributary-catchment denudation rates and the spatial distribution of litho-tectonic units within the DB area (Figs. 2 and 6). The highest denudation rates are observed for tributaries with widespread bedrock exposure of granites of the Mont Blanc External Massif and its Helvetic terrigenous to carbonate sedimentary cover (82%; DB01: 0.68 ± 0.05 mm/yr), or with abundant gneisses of the Gran Paradiso Internal Massif (40-70%; DB03, 04, 05: average denudation rate of 0.51 ± 0.02 mm/yr). Moderate denudation rates around 0.4 mm/yr are observed for catchments with dominant Austroalpine gneisses and eclogitic micaschists (55-80%; DB07, 13, 18: average denudation rate of 0.43 ± 0.03 mm/yr) or with abundant gneisses and schists of the Briançonnais basement (60-88%; DB14, 17: average denudation rate of 0.41 ± 0.01 mm/yr). The lowest denudation rates were obtained for tributaries dominated by meta-ophiolites and calcschists of the Piedmont units (50-100%; DB08, 09, 11, 16: average denudation rate of 0.28 ± 0.04 mm/yr) and by the terrigenous to carbonate Briançonnais metasedimentary cover (88%; DB19: 0.25 ± 0.02).



275

Figure 6: Tributary-catchment denudation rates (A) and relative proportion of litho-tectonic units within individual catchments (B). Colour code in (A) refers to the most abundant litho-tectonic unit in each individual catchment (see Figure 2 for spatial distribution of the different litho-tectonic units).

5. Discussion

280 5.1 Correction factors for catchment-wide ^{10}Be production and denudation rates

As reported in Table S2, the different correction factors for quartz-content, LIA-glacier cover and snow-shielding lead to 16-53% decrease in catchment ^{10}Be production and inferred denudation rates compared to uncorrected estimates (i.e. including only catchment-averaged topographic shielding and excluding areas with slope $<3^\circ$). Such correction factors build on several assumptions and have different implications for our catchment-wide denudation rate results that are discussed hereafter.

285 First, assuming Quaternary deposits as quartz-bearing lithologies is a first-order approximation, since deposits derived from mafic and carbonate-sedimentary bedrocks would bring no or minor quartz to the sediment routing system. However, distinguishing deposit provenance/lithology in this Alpine environment, with complex glacial/periglacial systems, would require detailed field investigation and mapping, which is beyond the scope of this work. Moreover, our calculations show that correction for quartz-content has only a minimal effect on catchment-averaged ^{10}Be production and denudation rates, with
 290 only up to 10% difference between uncorrected and corrected results thus overlapping within uncertainties.

Second, correction factors for LIA-glacier cover and snow shielding lead instead to significant decrease in catchment-averaged ^{10}Be production and thus denudation rates (up to 42 and 17%, respectively). Since sediments in sub-/proglacial environments can derive from periglacial erosion from bedrock walls/peaks and/or re-mobilization of previously exposed material (with non-zero ^{10}Be concentration, e.g. moraine deposits; Wittmann et al., 2007; Delunel et al., 2014; Guillon et al., 2015), assuming null
 295 ^{10}Be concentration input from areas covered by LIA glaciers might lead to overcorrections of our denudation rate results. Uncertainties are related also to the snow-shielding correction approach. The snow-shielding vs. elevation model reported by Delunel et al. (2020) has been calibrated on snow-water equivalent records of the Swiss and French Alps, which are wetter regions compare to the DB catchment (Isotta et al., 2014). Therefore, LIA-glacier cover and snow-shielding corrections may be overestimated for the DB catchments, especially for high-elevation tributaries. In particular, catchment DB01 shows the



300 maximum corrections for both LIA-glacier cover and snow shielding (42 and 17% respectively; Table S2) and consequently
relatively low output denudation rate compared to estimates obtained for catchments downstream along the main DB river
(DB02, 12, 10; Fig. 2), despite similar ^{10}Be concentrations (Fig. 3).
We therefore acknowledge that our corrected catchment-averaged ^{10}Be production and denudation rates (Table 1 and Fig. 2)
should be considered as minimum estimates, given the correction factors for LIA-glacier cover and snow shielding, in line
305 with the recent compilation over the entire European Alps (Delunel et al., 2020).

5.2 Controlling factors and processes on ^{10}Be -derived catchment denudation rates

Our ^{10}Be -derived denudation rates, varying between 0.2 and 0.9 mm/yr, fit broadly within the values obtained over the
European Alps, where 95% of the considered catchments yield denudation rate values <1.2 mm/yr and rates for the Western
Alps range between 0.1 and 1.2 mm/yr (Delunel et al., 2020). Correlations with topographic, environmental and geologic
310 metrics allowed us to identify potential controlling mechanisms for denudation-rate variability within the DB catchment, that
we discuss here in comparison with studies conducted in other Alpine sectors.

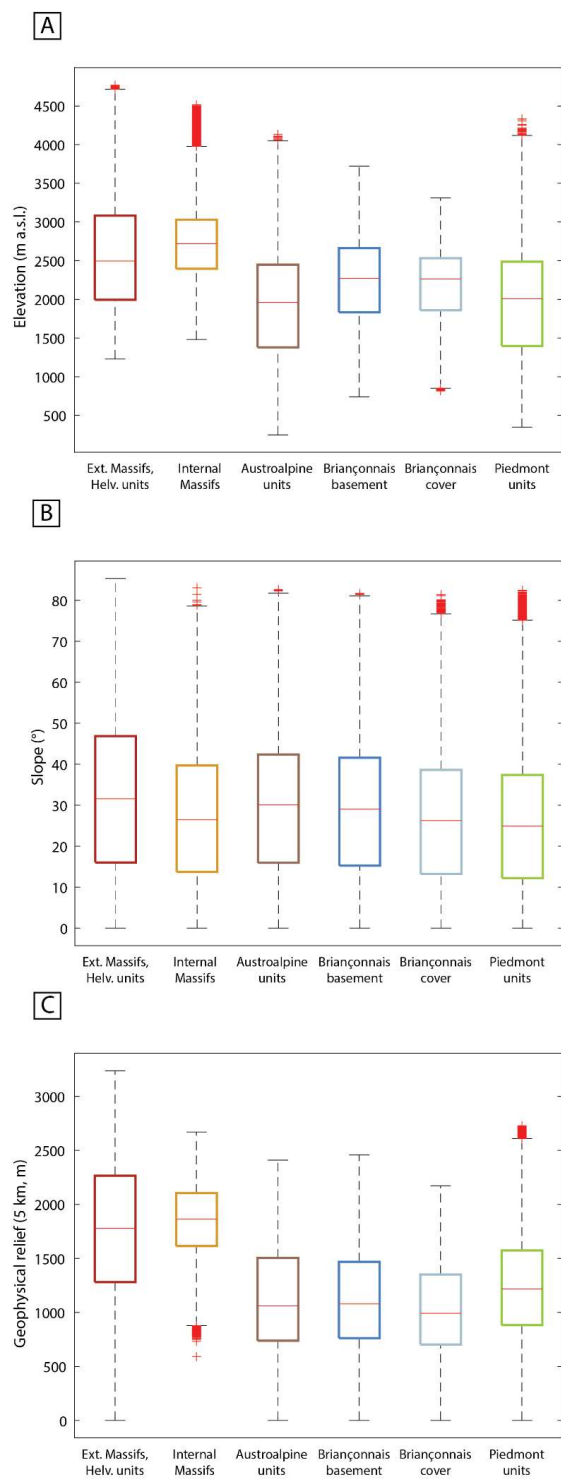
While precipitation and rock uplift have been recognized as main drivers for Alpine denudation rates, especially for the Central
Alps (e.g. Chittenden et al., 2014; Wittmann et al., 2007, respectively), their respective influence on denudation-rate variability
within DB is not significant (Figs. 5A and 4D). Interestingly, it can be observed that catchment geodetic rock uplift is higher
315 (20-80%) than ^{10}Be denudation in all the investigated tributary catchments, suggesting a net surface uplift of the DB area for
recent timescales, in line with other observations across the European Alps (Norton et al., 2011; Delunel et al., 2020).

Catchment topography, in turn conditioned by both bedrock erodibility and glacial overprint, appears instead to have a major
role in controlling the observed spatial variability in DB denudation rates. Denudation rates are indeed positively correlated
320 with catchment-averaged elevation and 5-km geophysical relief (Figs. 4A-C), and to a lesser extent with catchment averaged
slopes (i.e. when DB01 is included; Fig. 4B), similarly to what has been identified by previous studies. First, elevation
influences denudation rates through periglacial (i.e. frost-cracking; Delunel et al., 2010) and glacial erosive processes, both
increasing with elevation due to their temperature dependency, as well as by modifying soil and vegetation cover, with bare-
rock exposure being positively correlated with denudation rates (Fig. 5B). Second, topographic slope and relief are positively
325 correlated to catchment denudation until a threshold slope angle of 25-30° (Montgomery and Brandon, 2002; Champagnac et
al., 2014; Delunel et al., 2020). Below this threshold, denudation was shown to respond to a slope-dependent equilibrium
between regolith cover production through weathering and its downslope diffusion. In oversteepened catchments, denudation
rates are instead controlled by mass wasting processes (i.e. rockfalls, debris flows, landslides) which stochastically influence
river-sediment ^{10}Be concentrations. All the DB tributaries catchments have average slope comprised in the threshold range of
25-30°, with the exception of DB01 whose average slope is higher than 30°.

330 Our results also show a correlation between catchment denudation rates and bedrock litho-tectonic classification (Fig. 6),
which has been proposed to govern erosion through rock mechanical strength (erodibility; Kühni and Pfiffner, 2001). Similar
to what has been suggested for DB modern sediment provenance (Vezzoli et al., 2004), we observe a counter-intuitive trend
with the highest denudation rates in catchments dominated by apparent “low erodibility” bedrocks (granite and gneiss), and
the lowest rates in catchments with apparent “high erodibility” bedrocks (carbonate and terrigenous rocks; erodibility classes
335 according to Kühni and Pfiffner, 2001). This trend has already been observed locally in the Eastern and Southern Alps (Norton
et al., 2011) as well as at the scale of the entire European Alps (Delunel et al., 2020). Such observations were interpreted to be
related to the influence of bedrock resistance on catchments morphometry (in turn connected to erosion dynamics), with the
most resistant lithologies located at highest elevations and sustaining the steepest slopes/highest reliefs (Kühni and Pfiffner,
2001; Stutenbecker et al., 2016). To test this hypothesis at the scale of the DB catchment, we evaluated the distribution of
340 elevation, slope and 5-km geophysical relief for each individual litho-tectonic unit (Fig. 7). While the slope distributions appear
similar for all the different litho-tectonic domains (median of 26-31°; Fig. 7B), higher elevations and reliefs are observed for



the External and Internal Massifs (median elevation of 2500-2700 m a.s.l., median relief of around 1800 m; Fig. 7A) compared to the other litho-tectonic units (median elevation of 2000-2200 m a.s.l., median relief of 1000-1200 m; Fig. 7C). We tentatively suggest that the lithological control on DB denudation-rate variability (Fig. 6) is connected to the influence of bedrock erosional resistance on topography, with “low-erodibility” rocks supporting high-altitude and high-relief catchments where erosion processes’ efficiency promote high catchment denudation rates (Figs. 4A and C). Moreover, the different long-term tectonic histories of the litho-tectonic domains could also explain some of the observed variability in catchment denudation between areas west and east of the Penninic Frontal Thrust (Fig. 2). Bedrock tectonic fracturing (Molnar et al. 2007) may influence subsequent erodibility and denudation, facilitated by the exhumation of more fractured bedrock units such as the crystalline units of the Mont Blanc External Massif and its Helvetic sedimentary cover (no deep Eocene subduction during Alpine orogeny), compared to deeply-exhumed rocks of the Internal Massifs and Piedmont units (Schmid et al., 2004). Additionally, higher late-Miocene uplift rates in the Mont Blanc Massif compared to the rest of the DB catchment (Malusà et al., 2005) could have sustained high-elevations in the Mont Blanc Massif, which in turn would also promote high denudation rates. Lastly, we consider the potential connection between landscape glacial imprint and catchment denudation rates. Our correlations between catchment denudation rates and LGM glacial metrics (mean LGM ice-thickness and catchment proportion above LGM ELA, Table S3 and Fig. 5D) appear non-significant, suggesting no direct control of LGM glacial metrics on our calculated denudation rates. However, steep Alpine slopes and high reliefs are clear witnesses of Quaternary glacial erosion, and their significant correlation to denudation rates (Figs. 4B and C) is therefore indicative of a long-term topographic control on postglacial erosional response, as suggested by previous studies (Norton et al., 2010a; Glotzbach et al., 2013; Dixon et al., 2016). The glacial pre-conditioning of the topography has been also enhanced during postglacial times with coupled fluvial incision and hillslope processes increasing Alpine valley slopes and reliefs locally (Korup and Schlunegger, 2007; Valla et al., 2010; van den Berg et al., 2012). Over the shorter term, the positive correlation between catchment denudation rates and LIA glacial cover (only when including DB01, Fig. 5C) suggests an important role of Holocene to modern glacial processes in influencing catchment denudation, by contributing to high-sediment delivery (Stutenbecker et al., 2018). By considering the above-mentioned controlling mechanisms for catchment denudation, we propose an interpretation for the high denudation rate obtained for catchment DB01 compared to other DB tributaries (Fig. 2). Such an observation has already been suggested based on modern sediment provenance (Vezzoli et al., 2004; Vezzoli, 2004). Catchment DB01 has maximum values for most of the investigated metrics (Figs. 4 and 5, Table 2). Its location in the high-elevation core of the Alps (Mont Blanc Massif, long- and short-term high uplift rate) was the site of intense Quaternary glaciations (large catchment area above the LGM ELA), which deeply modified the landscape as illustrated by the high geophysical relief of this catchment. Thanks to the highly-resistant granitoid lithology, steep slopes and high reliefs deriving from glacial erosion could be maintained, in turn promoting high millennial to present-day denudation rates in this catchment. Finally, the supply of sediments by retreating glaciers and active periglacial processes, and the contribution of frequent rockfall events triggered by abundant precipitations (Fig. 5A) and present-day permafrost degradation (Ravanel et al., 2010; Akçar et al., 2012; Deline et al., 2015) participate to the significant sediment yield in the DB01 catchment. It thus supplies material with highly depleted ^{10}Be concentrations to the river system, which is in turn capable of significantly dilute the ^{10}Be signal along the DB course (Fig. 3, see following section for discussion).



380 **Figure 7:** Box-and-whisker plots for spatial distribution within the entire Dora Baltea catchment of elevation (A), slope (B), and 5-km geophysical relief (C), classified by individual litho-tectonic unit. Red line represents the median of each distribution, bottom and top of each box are the 25th and 75th percentiles. Whiskers extend up to 1.5 times the interquartile range, outliers (red crosses) are observations beyond the whiskers.



5.3 Propagation of ^{10}Be signal along the DB course

Our results highlight the strong ^{10}Be -dominance of catchment DB01 on downstream sediment samples collected along the DB course, below the tributary junctions (Fig. 3, Table 1). The constant low ^{10}Be concentrations measured for samples DB01, 02, 12, 10, 06 (around 1.2×10^4 at/g) indicate unequal sediment mixing (non-balanced sediment budget; Savi et al., 2014) between the main DB stream and the tributaries (^{10}Be concentrations of $2.0\text{--}4.9 \times 10^4$ at/g).

A key factor governing the mixing and flux balance of ^{10}Be concentrations between river streams is the quartz flux from each stream, which is in turn influenced by (1) catchment denudation rate, (2) drainage area, (3) catchment quartz content (Carretier et al., 2015), (4) sediment storage (e.g. dams, lakes, floodplains reducing mass flux but not changing the ^{10}Be concentration; Wittmann et al., 2016). Our results show significantly higher denudation rate for catchment DB01 compared to other DB tributaries (Fig. 2, Table 1). Moreover, the sediment-provenance study of Vezzoli (2004) highlighted that river sands from the Mont Blanc catchment (analogous catchment to DB01) have up to $\sim 20\%$ higher quartz content than other DB tributaries. Since the upstream catchment area of DB01 is comparable to most other DB tributaries (Table 2), and the presence of dams is limited to few catchments only (Fig. 1), we propose that the ^{10}Be -signal dominance of DB01 along the DB course comes from (1) its high denudation rate (Fig. 2 and Table 1) and (3) the high quartz content of the Mont Blanc granitoid (Vezzoli, 2004). The high rock-slope instability and glaciogenic sediment production in the Mont Blanc Massif supply low ^{10}Be concentration material to the river system, and are therefore efficient in diluting the ^{10}Be concentration in the downstream course of the DB river.

Following the approach reported in Delunel et al. (2014), we can obtain a first-order estimate of the relative contribution of the Mont Blanc Massif to the river-sediment ^{10}Be signal measured along the DB river. River-sediment ^{10}Be concentrations from tributaries and along the DB are first normalised to the SLHL ^{10}Be production rate (i.e. 4.18 ± 0.26 at $\text{g}^{-1} \text{yr}^{-1}$), implying that variations in normalised ^{10}Be concentrations represent the variability in denudation rates only. We then estimate the respective contributions of the Mont Blanc Massif and different tributaries through a mixing model considering 1) the normalised ^{10}Be concentration for river materials exported from the Mont Blanc catchment and 2) the averaged normalised ^{10}Be concentration from the upstream tributaries contributing to each sampling points along the main DB river. Between our two most upstream DB river samples (DB01 and DB02), we base our model on DB02, which provides a more conservative estimate of the contribution of the export from Mont Blanc catchment (i.e. the potential contributions of the tributaries are maximized while that of Mont Blanc catchment is minimized). By applying this simple model, we find that the Mont Blanc catchment contributes to $>77\%$ of the river-sediment ^{10}Be signal carried all along the DB river, while it only represents around 15% of the total DB catchment area (i.e. at DB06 sampling point). This first-order estimate further exemplifies the significant role of the Mont Blanc Massif in governing the sediment yield along the main DB river.

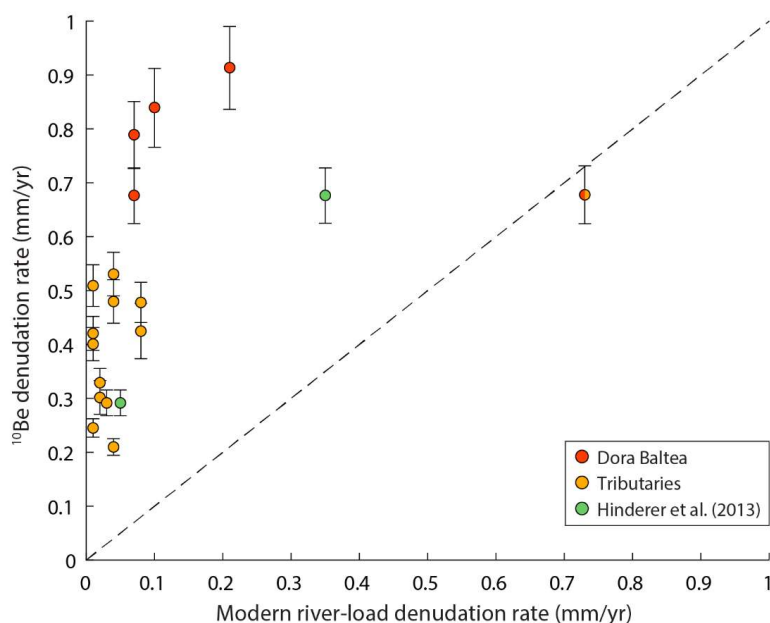
For the entire DB catchment, we can note that the ^{10}Be concentration is $\sim 30\%$ higher for sample T12 ($1.99 \pm 0.14 \times 10^4$ at/g; Wittmann et al., 2016) compared to DB06 ($1.52 \pm 0.08 \times 10^4$ at/g; Fig. 3), both collected at the same location (DB catchment outlet, Fig. 1) but at different time periods. The observed difference is probably related to a stochastic change in sediment sources (Lupker et al., 2012), with temporary dominant sediment input from a DB tributary catchment with higher ^{10}Be concentration (e.g. DB07, close location and similar ^{10}Be concentration as T12; Fig. 3) than from the Mont Blanc catchment. By comparing our results to the Po catchment (Wittmann et al., 2016), which drains several main river systems from the south-western Alps in addition to the DB river basin, it emerges that the low ^{10}Be concentration signal deriving from the Mont Blanc Massif, and remaining overall constant along the DB course, increases significantly soon after the DB flows into the Po river. The high ^{10}Be concentrations measured by Wittmann et al. (2016) in Po river-sediment samples, immediately downstream the DB confluence (samples P1 and P3: around 3.6×10^4 at/g), show that the Po river is dominated in its initial lowland flow by the high ^{10}Be concentration inputs from other south-western Alpine catchments (Wittmann et al., 2016).



5.4 Long- and short-term DB denudation rates

425 The general trend emerging from our ^{10}Be -derived denudation rates, of higher millennial denudation rates in the Mont Blanc Massif compared to other DB tributaries (Fig. 2), is overall in agreement (albeit with different absolute values) with erosion rate estimates on different timescales.

Long-term (10^6 - 10^7 yr) exhumation rates estimated from bedrock apatite fission-track dating (Malusà et al., 2005) show higher values (0.4-0.7 km/Myr) in the western sector of the DB catchment (west of Internal Houiller Fault, Fig. 2) than in the east (around 0.2 km/Myr, between the Internal Houiller and the Insubric Faults, Fig. 2). Likewise, results from detrital apatite fission-track dating (Resentini and Malusà, 2012) indicate that short-term (10^2 - 10^5 years) erosion rates are higher (around 0.5 mm/yr) in the Mont Blanc External Massif and its sedimentary cover (west of the Penninic Frontal Thrust) than in the axial belt, east of the Penninic Frontal Thrust (around 0.1 mm/yr; Fig. 2). Similarly to what has been shown by Glotzbach et al. (2013), the external Alps catchments (west of the Penninic Frontal Thrust; Fig. 2) appear to have equivalent long-term (apatite fission-track derived) and short-term (^{10}Be -derived) erosion rates, while internal Alps catchments (east of the Penninic Frontal Thrust; Fig. 2) have higher short-term than long-term erosion rates. This has been tentatively explained by potential differences in driver mechanisms of denudation before and during the Quaternary (Glotzbach et al., 2013). Tectonic forcing dominated Neogene denudation rates, with fast exhuming External Massifs having steeper rivers and higher reliefs and therefore eroding faster than the slowly-exhuming Internal Alpine Massifs. During the Quaternary, instead, climate fluctuations and associated glaciations modified both the Internal and External Alps morphology, also resulting in increasing denudation rates for the Internal Alps. Our ^{10}Be -derived catchment denudation rates are therefore not totally reflecting long-term exhumation rates over Myr timescales but most probably highlight Quaternary erosion dynamics.



445 **Figure 8:** Comparison of ^{10}Be - and modern river yield-derived catchment wide denudation rates. For all tributary catchments and DB locations, modern denudation rates derived from empirical estimates of river bedload are available (Vezzoli et al., 2004; red and yellow dots for DB and tributary catchments, respectively). For catchment DB06 and DB011, also modern denudation rates derived respectively from sediment gauging and sediment trapping are plotted in green (Hinderer et al., 2013, after Bartolini et al., 1996 and Bartolini and Fontanelli, 2009). Errors are represented only for ^{10}Be -derived denudation rates, since they are not reported for the modern rates.



Modern denudation rates, obtained from sediment-yield estimates (all DB catchments; Vezzoli et al., 2004; based on
450 Gavrilovic empirical formula, Gavrilovic, 1988) and measurements (sediment gauging for DB06 and sediment trapping for
DB11; Hinderer et al., 2003, after Bartolini et al., 1996 and Bartolini and Fontanelli, 2009), display higher values for samples
along the DB (0.07-0.73 mm/yr) compared to DB tributaries (0.01-0.08 mm/yr). While such a pattern is consistent with our
¹⁰Be-derived records, millennial denudation rates are 2 to 50 times greater than modern denudation rates, with the exception
of sample DB01 for which modern and ¹⁰Be denudation rates are roughly similar (Fig. 8). Equivalent order of discrepancy
455 between modern sediment-yield and ¹⁰Be-derived denudation rates has been observed by several studies (e.g. Kirchner et al.,
2001; Schaller et al., 2001; Wittmann et al., 2007, 2016; Stutenbecker et al., 2018). Among other factors, this discrepancy was
interpreted to point to the separate or combined effects of (1) incorporation in the ¹⁰Be-derived but not in the sediment-yield
denudation rates of high-magnitude low-frequency erosion events, (2) contribution of bedload and carbonate dissolution to
¹⁰Be-derived but not to sediment-yield denudation rates, (3) linear dissection of the landscape by fluvial erosion and subglacial
460 sediment export, leading to preferential erosion of material with low ¹⁰Be concentration, overestimating ¹⁰Be-derived
denudation rates, (4) sediment traps (e.g. lakes, dams), changing the flux measured by sediment gauging but less probably the
¹⁰Be concentration which is averaged over longer timescales. The first and third hypotheses could be the most plausible for
our results. Modern denudation rates are potentially not capturing the occurrence of large sporadic erosional events (Kirchner
et al., 2001; Schaller et al., 2001), with the exception of catchment DB01 (and therefore DB02, 06, 10, 12 along the main DB
465 course), where massive erosional events have been occurring during the Holocene towards present-day (i.e. rockfall events;
Deline et al., 2012, 2015) and therefore potentially included in the 10¹-10² yr integration time of the modern denudation rates.
Alternatively, low ¹⁰Be-concentration sediment input in the river system, coming from linear fluvial incision and subglacial
sediment export, could explain the mismatch between modern and millennial denudation rates, with ¹⁰Be-derived denudation
rates being potentially overestimated (Stutenbecker et al., 2018).

470 **Conclusions**

Our ¹⁰Be-derived catchment-wide denudation rates obtained in the Dora Baltea (DB) catchment (western Italian Alps) vary
between 0.2 and 0.9 mm/yr and fit within literature values across the European Alps (Delunel et al., 2020). Correlation of
output denudation rates with topographic, environmental and geologic metrics excludes any significant control of precipitation
and rock uplift on the observed variability in denudation rates within the DB catchment. Our results instead highlight the main
475 influence of catchment bedrock erodibility (litho-tectonic origin) and associated topographic metrics on denudation rate
variability among the 13 main tributaries. As previously supposed for some other parts of the Alps, our study shows that the
most resistant lithologies (granite and gneiss) support high-elevation and high-relief catchments where glacial and slope
processes are more intense and denudation rates are higher than in low-elevation/relief catchments, dominated by “high
erodibility” bedrocks (carbonate and terrigenous rocks).
480 This litho-tectonic control on catchment denudation is exemplified by the tributary catchment draining the Mont Blanc Massif,
which has the highest ¹⁰Be-derived denudation rate from our dataset and appears as an end-member for most of the investigated
metrics. Located in the long-term actively-uplifting core of the European Alps, the Mont Blanc Massif also experienced intense
Quaternary glaciations which deeply modified the landscape. Steep slopes and high reliefs could be supported by the highly-
resistant granitoid lithology, which in turn have been influencing the millennial to present-day high denudation of the
485 catchment, governed by intense glacial/periglacial processes and recurring rockfall events. In addition, our results also show
that the high sediment input from the Mont Blanc catchment dominates the DB sediment flux, contributing to >77% of the
¹⁰Be signal carried by river sediments along the DB main river, even downstream of multiple tributary junctions. This suggests
poor sediment mixing and balance between tributary fluxes along the DB catchment.



Finally, our ^{10}Be -derived denudation rates allow for comparison with long-term (10^6 - 10^7 yr, from thermochronology) and
490 modern (10^1 - 10^2 yr, from sediment budget) erosion rates, showing that, albeit different absolute values, the spatial trend in
catchment denudation is overall in agreement over different timescales, with higher millennial denudation rates in the Mont
Blanc Massif compared to the rest of the DB catchment.

Data availability

The data used in this study is available upon request.

495 Author contributions

ES, PGV and RD designed the study. ES, PGV and NG performed field investigations and sample collection. ES performed
 ^{10}Be cosmogenic sample preparation under supervisions of NA, ^{10}Be production/denudation rate calculation and analyses. MC
performed ^{10}Be measurements. RD performed ^{10}Be -budget calculations. ES wrote the manuscript with input from all co-
authors.

500 Acknowledgements

The authors warmly thank F. Magrani for the help during fieldwork. J. Krbanjevic is thanked for support for ^{10}Be sample
preparation. This study was supported by the Swiss National Science Foundation SNSF (Grant PP00P2_170559) and the
French ANR-PIA programme (ANR-18- MPGA-0006).

Competing interests

505 The authors declare no competing interests.

References

- Akçar, N., Deline, P., Ivy-Ochs, S., Alfimov, V., Hajdas, I., Kubik, P. W., Christl, M. and Schlüchter, C.: The AD 1717 rock
avalanche deposits in the upper Ferret Valley (Italy): A dating approach with cosmogenic ^{10}Be , *J. Quat. Sci.*, 27(4), 383–392,
doi:10.1002/jqs.1558, 2012.
- 510 Akçar N., Ivy-Ochs S., Alfimov V., Schlunegger F., Claude A., Reber R., Christl M., Vockenhuber C., Dehnert A., Meinert
R., and Schlüchter C.: Isochron-burial dating of glaciofluvial deposits: primary results from the Alps. *Earth Surface Processes
and Landforms*, 42, 2414–2425, <https://doi.org/10.1002/esp.4201>, 2017.
- Baroni, C., Gennaro, S., Cristina, M., Ivy-ochs, S., Christl, M., Cerrato, R. and Orombelli, G.: Last Lateglacial glacier advance
in the Gran Paradiso Group reveals relatively drier climatic conditions established in the Western Alps since at least the
515 Younger Dryas, *Quat. Sci. Rev.*, 255, 106815, doi:10.1016/j.quascirev.2021.106815, 2021.
- Bartolini, C. and Fontanelli, K.: Present versus long term sediment yield to the Adriatic Sea and the reliability of gauging
stations data, *Bollettino della Società Geologica Italiana* 128(3), 655–667, doi:10.3301/IJG.2009.128.3.655, 2009.
- Bartolini, C., Caputo, R. and Pieri, M.: Pliocene-Quaternary sedimentation in the Northern Apennine foredeep and related
denudation, *Geol. Mag.*, 133(3), 255–273, doi:10.1017/s0016756800009006, 1996.
- 520 von Blanckenburg, F.: The control mechanisms of erosion and weathering at basin scale from cosmogenic nuclides in river
sediment, *Earth Planet. Sci. Lett.*, 237(3–4), 462–479, doi:10.1016/j.epsl.2005.06.030, 2005.



- Bookhagen, B. and Strecker, M. R.: Spatiotemporal trends in erosion rates across a pronounced rainfall gradient: Examples from the southern Central Andes, *Earth Planet. Sci. Lett.*, 327–328, 97–110, doi:10.1016/j.epsl.2012.02.005, 2012.
- Brocklehurst, S. H. and Whipple, K. X.: Hypsometry of glaciated landscapes, *Earth Surf. Process. Landforms*, 29(7), 907–926, doi:10.1002/esp.1083, 2004.
- 525 Carretier, S., Regard, V., Vassallo, R., Martinod, J., Christophoul, F., Gayer, E., Audin, L. and Lagane, C.: A note on ¹⁰Be-derived mean erosion rates in catchments with heterogeneous lithology: Examples from the western Central Andes, *Earth Surf. Process. Landforms*, 40(13), 1719–1729, doi:10.1002/esp.3748, 2015.
- Champagnac, J. D., Schlunegger, F., Norton, K., von Blanckenburg, F., Abbühl, L. M. and Schwab, M.: Erosion-driven uplift of the modern Central Alps, *Tectonophysics*, 474(1–2), 236–249, doi:10.1016/j.tecto.2009.02.024, 2009.
- 530 Champagnac, J. D., Valla, P. G. and Herman, F.: Late-Cenozoic relief evolution under evolving climate: A review, *Tectonophysics*, 614, 44–65, doi:10.1016/j.tecto.2013.11.037, 2014.
- Charreau, J., Blard, P. H., Zumaque, J., Martin, L. C. P., Delobel, T. and Szafran, L.: Basinga: A cell-by-cell GIS toolbox for computing basin average scaling factors, cosmogenic production rates and denudation rates, *Earth Surf. Process. Landforms*, 44(12), 2349–2365, doi:10.1002/esp.4649, 2019.
- 535 Chittenden, H., Delunel, R., Schlunegger, F., Akçar, N. and Kubik, P.: The influence of bedrock orientation on the landscape evolution, surface morphology and denudation (¹⁰Be) at the Niesen, Switzerland, *Earth Surf. Process. Landforms*, 39(9), 1153–1166, doi:10.1002/esp.3511, 2014.
- Christl, M., Vockenhuber, C., Kubik, P. W., Wacker, L., Lachner, J., Alfimov, V. and Synal, H. A.: The ETH Zurich AMS facilities: Performance parameters and reference materials, *Nucl. Instruments Methods Phys. Res. Sect. B Beam Interact. with Mater. Atoms*, 294, 29–38, doi:10.1016/j.nimb.2012.03.004, 2013.
- 540 Clark, P.U., Dyke, A.S., Shakun, J.D., Carlson, A.E., Clark, J., Wohlfarth, B., Mitrovica, J.X., Hostetler, S.W., and McCabe, A.M.: The Last Glacial Maximum. *Science* 325, 710–4. <https://doi.org/10.1126/science.1172873>, 2009
- Codilean, A.T., 2006. Calculation of the cosmogenic nuclide production topographic shielding scaling factor for large areas using DEMs. *Earth Surf. Process. Landf.* 31(6), 785–794. <https://doi.org/10.1002/esp.1336>, 2006
- 545 Dal Piaz, G. V., Gianotti, F., Monopoli, B., Pennacchioni, G., Tartarotti, P. and Schiavo, A.: Carta Geologica d’Italia - Foglio 091, Chatillon, , 1–152, 2008.
- Deline P., Akçar N., Ivy-Ochs S., and Kubik P.W.: Repeated Holocene rock avalanches onto the Brenva Glacier, Mont Blanc massif, Italy: A chronology. *Quaternary Science Reviews*, 126, 186–200. <https://doi.org/10.1016/j.quascirev.2015.09.004>,
- 550 2015.
- Deline, P., Kirkbride, M. P., Ravello, L. and Ravello, M.: The Tré-la-Tête rockfall onto the Lex Blanche Glacier, Mont Blanc Massif, Italy, in September 2008, *Geogr. Fis. e Din. Quat.*, 31(2), 251–254, 2008.
- Deline, P., Gruber, S., Delaloye, R., Fischer, L., Geertsema, M., Giardino, M., Hasler, A., Kirkbride, M., Krautblatter, M., Magnin, F., McColl, S., Ravello, L. and Schoeneich, P.: Ice Loss and Slope Stability in High-Mountain Regions, Elsevier Inc., 2014.
- 555 Delunel, R., Van der Beek, P.A., Bourlès, D.L., Carcaillet, J. and Schlunegger, F. Transient sediment supply in a high-altitude Alpine environment evidenced through a ¹⁰Be budget of the Etages catchment (French Western Alps). *Earth Surface Processes and Landforms*, 39(7), 890–899, <https://doi.org/10.1002/esp.3494>, 2014.
- Delunel, R., van der Beek, P. A., Carcaillet, J., Bourlès, D. L. and Valla, P. G.: Frost-cracking control on catchment denudation rates: Insights from in situ produced ¹⁰Be concentrations in stream sediments (Ecrins-Pelvoux massif, French Western Alps), *Earth Planet. Sci. Lett.*, 293(1–2), 72–83, doi:10.1016/j.epsl.2010.02.020, 2010.
- 560 Delunel, R., Schlunegger, F., Valla, P. G., Dixon, J., Glotzbach, C., Hippe, K., Kober, F., Molliex, S., Norton, K. P., Salcher, B., Wittmann, H., Akçar, N. and Christl, M.: Late-Pleistocene catchment-wide denudation patterns across the European Alps, *Earth-Science Rev.*, 211, doi:10.1016/j.earscirev.2020.103407, 2020.



- 565 DiBiase, R. A., Heimsath, A. M. and Whipple, K. X.: Hillslope response to tectonic forcing in threshold landscapes, *Earth Surf. Process. Landforms*, 37(8), 855–865, doi:10.1002/esp.3205, 2012.
- Diolaiuti, G. A., Bocchiola, D., Vagliasindi, M., D’Agata, C. and Smiraglia, C.: The 1975-2005 glacier changes in Aosta Valley (Italy) and the relations with climate evolution, *Prog. Phys. Geogr.*, 36(6), 764–785, doi:10.1177/0309133312456413, 2012.
- 570 Dixon, J. L., Von Blanckenburg, F., Stüwe, K. and Christl, M.: Glaciation’s topographic control on Holocene erosion at the eastern edge of the Alps, *Earth Surf. Dyn.*, 4(4), 895–909, doi:10.5194/esurf-4-895-2016, 2016.
- Dunne, J., Elmore, D. and Muzikar, P.: Scaling factors for the rates of production of cosmogenic nuclides for geometric shielding and attenuation at depth on sloped surfaces, *Geomorphology*, 27(1–2), 3–11, doi:10.1016/S0169-555X(98)00086-5, 1999.
- 575 Glotzbach, C., Van Der Beek, P., Carcaillet, J. and Delunel, R.: Deciphering the driving forces of erosion rates on millennial to million-year timescales in glacially impacted landscapes: An example from the Western Alps, *J. Geophys. Res. Earth Surf.*, 118(3), 1491–1515, doi:10.1002/jgrf.20107, 2013.
- Hinderer, M., Kastowski, M., Kamelger, A., Bartolini, C. and Schlunegger, F.: River loads and modern denudation of the Alps - A review, *Earth-Science Rev.*, 118, 11–44, doi:10.1016/j.earscirev.2013.01.001, 2013.
- 580 Isotta, F. A., Frei, C., Weigluni, V., Perčec Tadić, M., Lassègues, P., Rudolf, B., Pavan, V., Cacciamani, C., Antolini, G., Ratto, S. M., Munari, M., Micheletti, S., Bonati, V., Lussana, C., Ronchi, C., Panettieri, E., Marigo, G. and Vertačnik, G.: The climate of daily precipitation in the Alps: Development and analysis of a high-resolution grid dataset from pan-Alpine rain-gauge data, *Int. J. Climatol.*, 34(5), 1657–1675, doi:10.1002/joc.3794, 2014.
- Kirchner, J. W., Finkel, R. C., Riebe, C. S., Granger, D. E., Clayton, J. L., King, J. G. and Megahan, W. F.: Mountain erosion over 10 yr, 10 k.y., and 10 m.y. time scales, *Geology*, 29(7), 591–594, doi:10.1130/0091-7613(2001)029<0591:MEOYKY>2.0.CO;2, 2001.
- 585 Korup, O. and Schlunegger, F. Bedrock landsliding, river incision, and transience of geomorphic hillslope-channel coupling: Evidence from inner gorges in the Swiss Alps. *Journal of Geophysical Research: Earth Surface*, 112(F3), <https://doi.org/10.1029/2006JF000710>, 2007.
- 590 Kober, F., Hippe, K., Salcher, B., Ivy-Ochs, S., Kubik, P. W., Wacker, L. and Hähnen, N.: Debris-flow-dependent variation of cosmogenically derived catchment-wide denudation rates, *Geology*, 40(10), 935–938, doi:10.1130/G33406.1, 2012.
- Kühni, A. and Pfiffner, O. A.: The relief of the Swiss Alps and adjacent areas and its relation to lithology and structure: Topographic analysis from a 250-m DEM, *Geomorphology*, 41(4), 285–307, doi:10.1016/S0169-555X(01)00060-5, 2001.
- Lupker, M., Blard, P. H., Lavé, J., France-Lanord, C., Leanni, L., Puchol, N., Charreau, J. and Bourlès, D.: ¹⁰Be-derived
- 595 Himalayan denudation rates and sediment budgets in the Ganga basin, *Earth Planet. Sci. Lett.*, 333–334, 146–156, doi:10.1016/j.epsl.2012.04.020, 2012.
- Malusà, M. G., Polino, R., Zattin, M., Bigazzi, G., Martin, S. and Piana, F.: Miocene to Present differential exhumation in the Western Alps: Insights from fission track thermochronology, *Tectonics*, 24(3), 1–23, doi:10.1029/2004TC001782, 2005.
- Martin, L. C. P., Blard, P.-H., Balco, G., Lavé, J., Delunel, R., Lifton, N. and Laurent, V.: The CREp program and the ICE-D
- 600 production rate calibration database: A fully parameterizable and updated online tool to compute cosmic-ray exposure ages, *Quat. Geochronol.*, 38, 25–49, doi:10.1016/J.QUAGEO.2016.11.006, 2017.
- Maxeiner, S., Synal, H. A., Christl, M., Suter, M., Müller, A. and Vockenhuber, C.: Proof-of-principle of a compact 300 kV multi-isotope AMS facility, *Nucl. Instruments Methods Phys. Res. Sect. B Beam Interact. with Mater. Atoms*, 439(November 2018), 84–89, doi:10.1016/j.nimb.2018.11.028, 2019.
- 605 Moon, S., Page Chamberlain, C., Blisniuk, K., Levine, N., Rood, D. H. and Hilley, G. E.: Climatic control of denudation in the deglaciated landscape of the Washington Cascades, *Nat. Geosci.*, 4(7), 469–473, doi:10.1038/ngeo1159, 2011.



- Muscheler, R., Beer, J., Kubik, P. W. and Synal, H. A.: Geomagnetic field intensity during the last 60,000 years based on ^{10}Be and ^{36}Cl from the Summit ice cores and 14C, *Quat. Sci. Rev.*, 24(16–17), 1849–1860, doi:10.1016/j.quascirev.2005.01.012, 2005.
- 610 Norton, K. P., Abbühl, L. M. and Schlunegger, F.: Glacial conditioning as an erosional driving force in the Central Alps, *Geology*, 38(7), 655–658, doi:10.1130/G31102.1, 2010.
- Norton, K. P., von Blanckenburg, F., DiBiase, R., Schlunegger, F. and Kubik, P. W.: Cosmogenic ^{10}Be -derived denudation rates of the Eastern and Southern European Alps, *Int. J. Earth Sci.*, 100(5), 1163–1179, doi:10.1007/s00531-010-0626-y, 2011.
- Perello, P., Gianotti, F. and Monopoli, B.: Carta Geologica d'Italia - Foglio 089, Courmayeur, 2008.
- 615 Polino, R., Malusà, M. G., Martin, S., Carraro, F., Gianotti, F. and Bonetto, F.: Carta Geologica d'Italia - Foglio 090, Aosta, , (3), 2008.
- Portenga, E. W. and Bierman, P. R.: Understanding earth's eroding surface with ^{10}Be , *GSA Today*, 21(8), 4–10, doi:10.1130/G111A.1, 2011.
- Ravello, L., Allignol, F., Deline, P., Gruber, S. and Ravello, M.: Rock falls in the Mont Blanc Massif in 2007 and 2008, *Landslides*, 7(4), 493–501, doi:10.1007/s10346-010-0206-z, 2010.
- 620 Resentini, A. and Malusà, M. G.: Sediment budgets by detrital apatite fission-Track dating (Rivers Dora Baltea and Arc, Western Alps), *Spec. Pap. Geol. Soc. Am.*, 487(08), 125–140, doi:10.1130/2012.2487(08), 2012.
- Sarmiento, J. L., Gruber, N., Brzezinski, M. A. and Dunne, J. P.: High-latitude controls of thermocline nutrients and low latitude biological productivity, *Nature*, 427(6969), 56–60, doi:10.1038/nature02127, 2004.
- 625 Savi, S., Norton, K., Picotti, V., Brardinoni, F., Akçar, N., Kubik, P. W., Delunel, R. and Schlunegger, F.: Effects of sediment mixing on ^{10}Be concentrations in the Zielbach catchment, central-eastern Italian Alps, *Quat. Geochronol.*, 19, 148–162, doi:10.1016/j.quageo.2013.01.006, 2014.
- Schaller, M., Von Blanckenburg, F., Hovius, N. and Kubik, P. W.: Large-scale erosion rates from in situ-produced cosmogenic nuclides in European river sediments, *Earth Planet. Sci. Lett.*, 188(3–4), 441–458, doi:10.1016/S0012-821X(01)00320-X, 630 2001.
- Schmid, S.M., Fügenschuh, B., Kissling, E., Schuster, R.: Tectonic map and overall architecture of the Alpine orogen. *Eclogae Geologicae Helvetiae*, 97(1), 93–117, doi: 10.1007/s00015-004-1113-x, 2004.
- Schwanghart, W. and Scherler, D.: Short Communication: TopoToolbox 2 - MATLAB-based software for topographic analysis and modeling in Earth surface sciences, *Earth Surf. Dyn.*, 2(1), 1–7, doi:10.5194/esurf-2-1-2014, 2014.
- 635 Serra, E., Valla, P.G., Gribenski, N., Carcaillet, Deline, P., in revision. Post-LGM glacial and geomorphic evolution of the Dora Baltea valley (western Italian Alps). *Quat. Sci. Rev.*
- Small, E. E. and Anderson, R. S.: Pleistocene relief production in Laramide mountain ranges, western United States:, *Geology*, 26(2), 123–126, doi:10.1130/0091-7613(1998)026<1150:PRPILM>2.3.CO;2, 1998.
- Sternai, P., Sue, C., Husson, L., Serpelloni, E., Becker, T. W., Willett, S. D., Faccenna, C., Di Giulio, A., Spada, G., Jolivet, 640 L., Valla, P., Petit, C., Nocquet, J. M., Walpersdorf, A. and Castelltort, S.: Present-day uplift of the European Alps: Evaluating mechanisms and models of their relative contributions, *Earth-Science Rev.*, 190(July 2018), 589–604, doi:10.1016/j.earscirev.2019.01.005, 2019.
- Stutenbecker, L., Costa, A. and Schlunegger, F.: Lithological control on the landscape form of the upper Rhône Basin, Central Swiss Alps, *Earth Surf. Dyn.*, 4(1), 253–272, doi:10.5194/esurf-4-253-2016, 2016.
- 645 Stutenbecker, L., Delunel, R., Schlunegger, F., Silva, T. A., Šegvić, B., Girardclos, S., Bakker, M., Costa, A., Lane, S. N., Loizeau, J. L., Molnar, P., Akçar, N. and Christl, M.: Reduced sediment supply in a fast eroding landscape? A multi-proxy sediment budget of the upper Rhône basin, Central Alps, *Sediment. Geol.*, 375, 105–119, doi:10.1016/j.sedgeo.2017.12.013, 2018.



- Uppala, S. M., Källberg, P. W., Simmons, A. J., Andrae, U., da Costa Bechtold, V., Fiorino, M., Gibson, J. K., Haseler, J.,
650 Hernandez, A., Kelly, G. A., Li, X., Onogi, K., Saarinen, S., Sokka, N., Allan, R. P., Andersson, E., Arpe, K., Balmaseda, M.
A., Beljaars, A. C. M., van de Berg, L., Bidlot, J., Bormann, N., Caires, S., Chevallier, F., Dethof, A., Dragosavac, M., Fisher,
M., Fuentes, M., Hagemann, S., Hólm, E., Hoskins, B. J., Isaksen, I., Janssen, P. A. E. M., Jenne, R., McNally, A. P., Mahfouf,
J. F., Morcrette, J. J., Rayner, N. A., Saunders, R. W., Simon, P., Sterl, A., Trenberth, K. E., Untch, A., Vasiljevic, D., Viterbo,
P. and Woollen, J.: The ERA-40 re-analysis, *Q. J. R. Meteorol. Soc.*, 131(612), 2961–3012, doi:10.1256/qj.04.176, 2005.
- 655 Valla, P. G., van der Beek, P. A. and Carcaillet, J.: Dating bedrock gorge incision in the French Western Alps (Ecrins-Pelvoux
massif) using cosmogenic ^{10}Be , *Terra Nov.*, 22(1), 18–25, doi:10.1111/j.1365-3121.2009.00911.x, 2010.
- Valla, P. G., Shuster, D. L. and Van Der Beek, P. A.: Significant increase in relief of the European Alps during mid-Pleistocene
glaciations, *Nat. Geosci.*, 4(10), 688–692, doi:10.1038/ngeo1242, 2011.
- Van den Berg, F., Schlunegger, F., Akçar, N. and Kubik, P.: ^{10}Be -derived assessment of accelerated erosion in a glacially
660 conditioned inner gorge, Entlebuch, Central Alps of Switzerland. *Earth Surface Processes and Landforms*, 37(11), 1176–1188,
<https://doi.org/10.1002/esp.3237>, 2012.
- Vezzoli, G.: Erosion in the Western Alps (Dora Baltea Basin): 2. Quantifying sediment yield, *Sediment. Geol.*, 171(1–4), 247–
259, doi:10.1016/j.sedgeo.2004.05.018, 2004.
- Vezzoli, G., Garzanti, E. and Monguzzi, S. Erosion in the western Alps (Dora Baltea basin): 1. Quantifying sediment
665 provenance. *Sedimentary Geology*, 171(1–4), 227–246, <https://doi.org/10.1016/j.sedgeo.2004.05.017>, 2004.
- Wittmann, H., von Blanckenburg, F., Kruesmann, T., Norton, K. P. and Kubik, P. W.: Relation between rock uplift and
denudation from cosmogenic nuclides in river sediment in the Central Alps of Switzerland, *J. Geophys. Res. Earth Surf.*,
112(4), 1–20, doi:10.1029/2006JF000729, 2007.
- Wittmann, H., Malusà, M. G., Resentini, A., Garzanti, E. and Niedermann, S.: The cosmogenic record of mountain erosion
670 transmitted across a foreland basin: Source-to-sink analysis of in situ ^{10}Be , ^{26}Al and ^{21}Ne in sediment of the Po river catchment,
Earth Planet. Sci. Lett., 452, 258–271, doi:10.1016/j.epsl.2016.07.017, 2016.
- Miller, B. B. and Carter, C.: The test article, *J. Sci. Res.*, 12, 135–147, doi:10.1234/56789, 2015.
- Smith, A. A., Carter, C., and Miller, B. B.: More test articles, *J. Adv. Res.*, 35, 13–28, doi:10.2345/67890, 2014.